Received May 21, 2020, accepted May 30, 2020, date of publication June 3, 2020, date of current version July 15, 2020.

Digital Object Identifier 10.1109/ACCESS.2020.2999748

Modelling and Simulation of Aerostatic Thrust Bearings

MUHAMMAD PUNHAL SAHTO[1,3], WEI WANG[1], MUHAMMAD IMRAN[2], LINSHAN HE[1], HAI LI[1], AND GONG WEIWEI[1]

[1]School of Mechanical and Electrical Engineering, University of Electronic Science and Technology of China, Chengdu 611731, China
[2]School of Engineering and Applied Science, Aston University, Birmingham B4 7ET, U.K.
[3]Department of Mechanical Engineering, The University of Lahore, Lahore 54590, Pakistan

Corresponding author: Wei Wang (wangwhit@163.com)

This work was supported in part by the National Natural Science Foundation, and in part by the National Association Security Foundation China (NASF) under Grant U183010027.

ABSTRACT This paper demonstrates the modelling and simulation comparison of the static characteristics of a porous, orifice, and multiple type aerostatic thrust bearings on the basis of load-carrying capacity(LCC) and stiffness. The equations Navier-Stokes (N-S) are used to solve the internal distribution of pressure in computational fluid dynamics(CFD) simulation environment. An axisymmetric model, which minimizes the computational time and increases efficiency, is used to evaluate the static characteristics of a porous, orifice, and multiple restrictors of aerostatic bearings. Our numerical analysis and empirical results show the agreement with the significant effect of material and geometrical parameters on the LCC and stiffness. The thickness of the air film is less than 10μm, the multiple orifice restrictors have more LCC than porous and orifice restrictor. The porous restrictor's stiffness is larger than orifice and multiple restrictors. The LCC of porous and orifice is notably smaller than multiple orifice restrictors. Additionally, it is analyzed that LCC of porous, orifice, and multiple orifice restrictors can be improved with an increase in the supply of air pressure.

INDEX TERMS Orifice, porous material, thrust bearings, static characteristics.

I. INTRODUCTION

TThe aerostatic bearings are used to acquire motion accuracy and minimum friction in numerous measuring machines, lithography equipment, and machine tools. Several kinds of restrictors such as porous, orifice, compound and slot usually used in aerostatic bearings. The porous bearing has an advantage over other restrictors because of its uniform pressure distribution on the surface of bearing. Due to this property, it has more force, stiffness, and stability, which are sustained by the porous material. Several studies have been initiated for finding characteristics of aerostatic bearings. Uichiro Nishuo *et al.* [1] has examined the characteristics of aerostatic bearing experimentally and numerically. The co-efficient of discharge can be numerically found out based on CFD using a finite difference method (FDM). The co-efficient of damping and stiffness of restrictors with feed-holes are larger than compound restrictors of bearings. Cui *et al.* [2] carried out a study on the pressure distribution of film, affected the porous aerostatic bearings by manufacturing errors. Zhanga *et al.* [3] analyzed that the depression of pressure is debilitated by increasing the diameter of orifice, minimizing the film thickness and pressure supply. Huanga *et al.* [4] exploit FDM and iterative processes to calculate static characteristics with vacuum pre-load thrust aerostatic bearing. Yoshimoto and Kohno [5] proposed two air supply methods of annular groove and hole supply to refrain from the deflection. A theoretical study by Li and Ding [6] showed that the performance of bearing is affected by the pressure of a gas, film thickness, structural design, and diameter of the orifice. They used FDM and iterative algorithm to minimize iterative times for calculating static characteristics with vacuum pre-load thrust aerostatic bearing. Numerous studies on orifice restrictor and porous thrust bearings provide detailed insights in terms of the impacts on LCC of different restrictors, and aerostatic bearing's stiffness. Schenk *et al.* [7] investigated the effect of gap height and gas load at the vacuum conditions to cause gas flow leakage. Jeng and Chang [8] examined stiffness with a comparison of single and double pad aerostatic bearings. Another study by Cui *et al.* [9], showed that the amplitude errors could arise with the variation of stiffness and load. The static performance of bearing improves with a porous thickness, which is

The associate editor coordinating the review of this manuscript and approving it for publication was Hamid Mohammad-Sedighi.

from 6-8mm when the film thickness decreases. The performance comparison study [10] of concave errors of the static characteristics with the convex error of the working surface are better. Moreover, Cui *et al.* [11] proposed proportional division method (PDM) and finite element method (FEM) to calculate the angular stiffness. It shows that suitable film thickness corresponds by increasing the diameter of orifice. The CFD is adopted to examine the discharge co-efficient without a feed pocket of the feed hole. The material thickness, air supply, and Young's modulus have a significant effect on the porous material, and they proposed double-layered porous restrictor. [12] The FDM method [13] is employed for the analysis of bearing's characteristics. Wen-Jong Lin *et al.* [14] also investigated the gas supply, orifice diameter, and bearing surface are the main elements for the performance of air bearing. As compared to the other types of aerostatic bearings, the porous aerostatic bearing has better performance in applications of high precision or speed [7], [15], [16]. Mathematical methods for source and slip flow are applied to calculate the static characteristics of aerostatic porous bearings [17]. According to D'Arcy law [18], the porous material in which the flow is taken parallel through a surface of bearing. As a little drop of gas at the inlet, stiffness improved with multiple restrictors of aerostatic bearings [19]. The study [20] shows that the proper arrangement of the plate and porosity parameters yield accelerated motion because of parameters of viscosity. An enhanced reduced-order modelling method [21] based on the proper orthogonal decomposition is proposed to obtain a dynamic system. The combination of the quasi-linearization method [22] is used to augment the strength of the electromagnetic field due to the boundary layer flow of an Eyring-Powell non-Newtonian fluid. A study proposes a semi-analytical [23] approach to investigate the steady 3D boundary layer flow of a SiC-TiO2/DO hybrid nanofluid over a porous spinning disk subject to a constant vertical magnetic field. The non-linear steady, [24] hydromagnetic micropolar flow is examined with radiation and heat source/sink effects which suggest that surface temperature magnetic field parameters increase microrotation. The literature review indicates that there have been individual studies on porous thrust and orifice restrictor type bearings and provides detailed insight into the impacts of different restrictors on LCC, and stiffness of aerostatic bearings. However, to the best of our knowledge, the *comparison between porous thrust and orifice restrictor* type bearing has not yet been reported.

In this paper, we investigate the porous restrictors, orifice, and multiple orifice restrictors. We also compare the stiffness and LCC of aerostatic porous thrust bearings. The LCC and stiffness are determined with internal distribution of pressure; the fluent CFD is used for internal distribution of pressure in the clearance of bearing. The impacts of supply pressure, a diameter of orifice, air film thickness, parameters of the material, and on LCC, and stiffness of the porous thrust aerostatic bearings are investigated. We find that an axisymmetric method is effective to minimize time and increase efficiency during the simulation process. The simulation results are validated with experiments. The remaining parts of the paper are arranged in the following sequence, consisting of several tasks as follows: The numerical modelling sections present the design and mathematical calculation of porous, orifice, and multiple restrictors aerostatic thrust bearings. The performance of bearing is evaluated in the section of modelling for different parameters. The permeability of porous material and load are tested in a section of an experimental setup. The simulated results of the porous, orifice, and multiple aerostatic thrust bearings are validated with experimental results in the section of experimental verification with numerical analysis.

TABLE 1. Nomenclature.

Symbol	Description
μ	the kinematic viscosity
α	the permeability co-efficient
$\bigtriangledown p$	the change in pressure
$\overrightarrow{u}$	the vector of velocity
x, y, z	the coordinates of porous section
$\alpha_{xj}, \alpha_{yj}, \alpha_{zj}$	permeability co-efficient of porous coordinates
$\Delta H_x, \Delta H_y, \Delta H_z$	the porous material thicknesses
$\Delta p_x, \Delta p_y, \Delta p_z$	the pressure drop in three directions x, y, z
u_j	the velocity
γ	the porosity
ρ	the density of the gas
t	the time
F_x	force on body in the x direction
F_y	force on body in the y direction
F_z	force on body in the z direction
k	co-efficient of heat transfer of fluid
$10\ gradT$	the gradient of temperature
c_p	the specific heat capacity
S	viscous dissipation energy
P_s	the pressure supply
P_d	outlet pressure
P_a	the atmospheric pressure
m_r	the rate of mass flow
C_d	the co-efficient of discharge
ψ_s	the function mass flow

II. NUMERICAL MODELLING

This section discusses the preliminaries, including restrictors construction, governing equations, and mass flow rate.

A. RESTRICTORS CONSTRUCTION

The ANSYS workbench is used to establish the finite element of the thrust bearing. The key object of fluent software is performing fluid simulation, as gas is flowing in the bearing, which is composed of two parts: gas film and porous. The basic geometric design of porous restrictors, orifice, and multiple restrictors are depicted in Fig 1. Through a porous material, gas flows to the film of bearing with a supply of pressure, and leaves out from an edge of the film to the

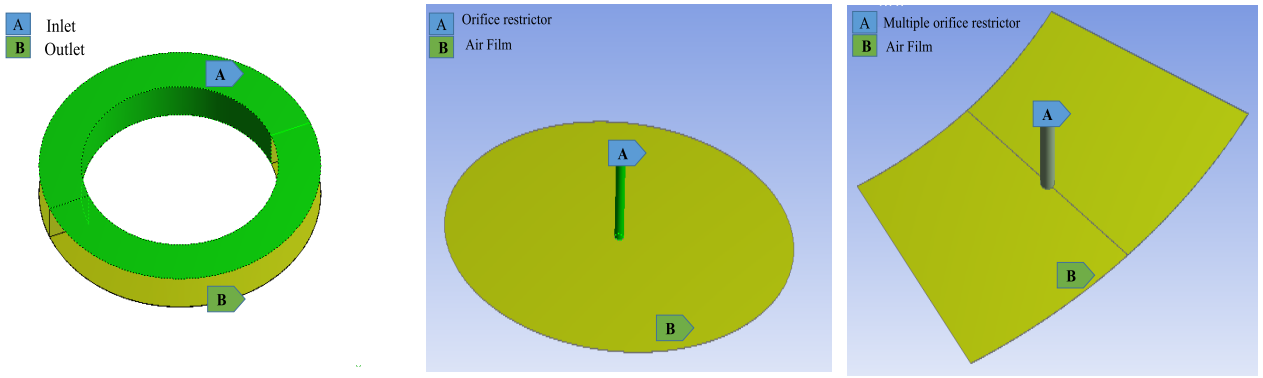

(a) (b) (c)

FIGURE 1. Geometrical construction of different types of restrictors.

atmosphere, as illustrated in Fig 1a. To support the pad, the thrust film was applied, the load capacity of bearing was determined by the film thickness. By way of the orifice and multiple restrictors, gas flows to the film and outflows to the atmosphere, as depicted in Fig 1b and 1c, respectively.

B. GOVERNING EQUATIONS

The pressure distribution calculation is of two parts of porous and the gas film. In the porous material, flow is viscous laminar, and according to Darcy - Forchheimer law, pressure drops as below.

$$\nabla p = -\frac{\mu \bar{u}}{\alpha} \tag{1}$$

where μ is a kinematic viscosity, α is the permeability co-efficient, ∇p is the change in pressure, and $\bar{u}$ is the vector of velocity.

The change in pressure of x, y, z coordinates of the porous section is:

$$\begin{aligned} \nabla p_x &= \sum_{j=1}^{3} \frac{\mu \bar{u}_j \Delta H_x}{\alpha_{xj}} \\ \nabla p_y &= \sum_{j=1}^{3} \frac{\mu \bar{u}_j \Delta H_y}{\alpha_{yj}} \\ \nabla p_z &= \sum_{j=1}^{3} \frac{\mu \bar{u}_j \Delta H_z}{\alpha_{zj}} \end{aligned} \tag{2}$$

where, α_{xj}, α_{yj}, α_{zj} are the porous material's co-efficient of permeability in the coordinates. The ΔH_x, ΔH_y, ΔH_z are the thicknesses of porous material in the three directions ∇p_x, ∇p_y, ∇p_z are the pressure drop in three directions x, y, z and $\bar{u}_j$ is the velocity in three coordinate directions.

In this paper, the permeability of porous material was taken as isotropic in the manufacturing process, as the cold isostatic pressing was conducted. It means that $\alpha_{xj}, \alpha_{yj}, \alpha_{zj}$ have similar values.

The conservation laws of momentum and mass are given below:

$$\frac{\partial(\gamma\rho)}{\partial t} + \mathrm{div}(\gamma\rho\vec{u}) = 0 \tag{3}$$

$$\frac{\partial(\gamma\rho u)}{\partial t} + \mathrm{div}(\gamma\rho\vec{u} \times u) = -\gamma \nabla p \tag{4}$$

As γ is the porosity, the density of the gas is ρ, and t is the time.

The fluid motion is mostly governed by conservation laws of mass, energy, and momentum in fluid mechanics, which can be formed by N-S equations. The continuity equation is also familiar as the conservation law of mass, is given as:

$$\frac{\partial \rho}{\partial t} + \frac{\partial(\rho u)}{\partial x} + \frac{\partial(\rho v)}{\partial y} + \frac{\partial(\rho w)}{\partial z} = 0 \tag{5}$$

$$\frac{\partial \rho}{\partial t} + \mathrm{div}(\rho\vec{u}) = 0 \tag{6}$$

where, ρ is the gas density, t is time, and $\bar{u}$ is the vector velocity of cartesian coordinates (x, y, and z), components of velocity u, v, and w are in the 3 coordinate directions. As Newton's second law states, that the equation for conservation of momentum in directions of x, y, z is derived as:

$$\begin{cases} \dfrac{\partial(\rho u)}{\partial t} + div(\rho\vec{u}u) = -\dfrac{\partial p}{\partial x} + \dfrac{\partial \tau_{xx}}{\partial x} + \dfrac{\partial \tau_{yx}}{\partial y} + \dfrac{\partial \tau_{zx}}{\partial z} + F_x, \\ \dfrac{\partial(\rho v)}{\partial t} + \mathrm{div}(\rho\vec{u}v) = -\dfrac{\partial p}{\partial y} + \dfrac{\partial \tau_{xy}}{\partial x} + \dfrac{\partial \tau_{yy}}{\partial y} + \dfrac{\partial \tau_{zy}}{\partial z} + F_y, \\ \dfrac{\partial(\rho w)}{\partial t} + div(\rho u w) = -\dfrac{\partial p}{\partial z} + \dfrac{\partial \tau_{xz}}{\partial x} + \dfrac{\partial \tau_{yz}}{\partial y} + \dfrac{\partial \tau_{zz}}{\partial z} + F_z \end{cases} \tag{7}$$

Here, ρ is the density of a gas, τ is the viscous fluid stress, F_x is the force towards x-direction, F_y is a force on the body towards y-direction, and F_z is the force on the body towards z direction.

The τ is proportional to the fluid deformation, derived as [25]:

$$\begin{cases} \tau_{xx} = 2\mu\dfrac{\partial u}{\partial x} + \lambda div(\vec{u});\ \tau_{xy} = \tau_{yx} = \mu\left(\dfrac{\partial u}{\partial y} + \dfrac{\partial v}{\partial x}\right) \\ \tau_{yy} = 2\mu\dfrac{\partial v}{\partial x} + \lambda div(\vec{u});\ \tau_{xz} = \tau_{zx} = \mu\left(\dfrac{\partial u}{\partial z} + \dfrac{\partial w}{\partial x}\right) \\ \tau_{zz} = 2\mu\dfrac{\partial w}{\partial x} + \lambda div(\vec{u});\ \tau_{yz} = \tau_{zy} = \mu\left(\dfrac{\partial u}{\partial z} + \dfrac{\partial w}{\partial y}\right) \end{cases} \quad (8)$$

where dynamic viscosity is μ, and $\lambda = -\frac{2}{3}$.

According to the thermodynamics 1st law, the law of energy conservation is given by:

$$\frac{\partial(\rho T)}{\partial t} + \mathrm{div}(\rho\vec{u}T) = \mathrm{div}\left(\frac{k}{c_p}\,\mathrm{grad}\,T\right) + \mathrm{S} \quad (9)$$

where k is the co-efficient of heat transfer of fluid, $gradT$ is the gradient of temperature, specific heat capacity is c_p, and viscous dissipation energy is S.

By solving equations 6, 7, 8, and 9, the distribution of pressure in the clearance of bearing of orifice restrictors can be gained. The distribution of pressure of porous thrust aerostatic bearings can be attained by solving equations, 1,2,3,4, and 9.

C. THE RATE OF MASS FLOW THROUGH AN ORIFICE

The configuration of the aerostatic thrust bearing, in which the orifices are used as restrictors. One row of orifices is evenly and equally spaced put around the bearing circumference. Taking into account, the flow through an orifice, bellow suppositions have been obtained [26]:

- The losses are not of upstream pressure of the jet throat, i.e., the p_s is supply pressure of jet at entry.
- The static pressure of the jet in the throat quickly goes down.

In general, the rate of mass flow of gas through the orifice is produced as an ideal nozzle. Since the pressure supply p_s is decreased p_d through an orifice. Derived from the ideal mass flow rate [27]:

$$m_r = C_d \times m_t \quad (10)$$

$$m_r = AP_S\sqrt{\frac{2\rho a}{P_a}\Psi_r} \quad \because A = \frac{\pi d^2}{4} \quad (11)$$

where P_a is the atmospheric pressure. d is the diameter of orifice, P_d is the outlet pressure of orifice, P_s is the pressure supply, specific heat ratio is the k, and $k = 1.4$ is the value for gas, ρ is the gas density, in actual condition m_r is the rate of mass flow, m_t is the theoretical rate of mass flow, and C_d is the co-efficient of discharge. And Ψ_s is the function of mass flow and is described as bellow:

$$\Psi_s = \begin{cases} \left[K/2(2/K+1)^{(K+1)/(K-1)}\right]^{1/2}; \\ \mathrm{P_d}/P_s \le (2/K+1)^{K/(K+1)} \\ \\ \left\{K/K-1\left[(P_d/P_s)^{2/k} - (P_d/P_s)^{(k+1)/k}\right]\right\}^{1/2}, \\ P_d/P_s > (2/K+1)^{K/(K+1)} \end{cases} \quad (12)$$

By solving equations (10)-(12), the flow of gas mass through an orifice can be obtained. Fig 2 shows a flow chart, calculation of static characteristics of a thrust bearing.

III. METHOD OF CALCULATION

Characteristics of flow field calculated of aerostatic bearings by using key methods that are FEM and FDM [28]. However, FEM and FDM cannot effectively solve the N-S equations. In this article, based on the CFD, FLUENT 16.0 is used to resolve N-S equations. The fluent is selected to calculate the equations for viscous laminar. In this research, the mass flow rate is minimal through porous. Hence, the model is a laminar described in the viscous state. An axisymmetric model is used to minimize the time during a simulation. The simulation is performed on NVIDIA Quadro K620-GPU(GM107) using memory 112GB.

A. GRIDS CALCULATION

In numerous antecedent research, the aerostatic pad bearings design was made simple to the symmetric model [29]. The boundary conditions and grids utilized for porous and orifice restrictors are shown in Fig 3.

The gas supplies through porous and outflows from film thickness to the atmosphere, as indicated at A and B, respectively. The C and D show the porous material through which gas supplies. An air film is shown at E and F respectively. In the orifice and multiple restrictors, the inlet, outlet, and air film are shown at A, B, and C, respectively. In CFD numerical simulation, the quality and number of grids have a significant influence on the simulation time and results. Therefore, the simulation time must be shortened, and the simulation output improved while ensuring the grid quality, the accuracy of the simulation results, and machine resources. The grid of porous material and film is divided into three directions: axial, circumferential, and radial (a, c, r). In this paper, for the minimizing time, and to increase the computation efficacy, the axisymmetric model is applied to evaluate characteristics of a porous, orifice, and multiple restrictors aerostatic circular pad bearings, as depicted in Fig 3a, 3b, 3c, respectively. The consideration of bearing mesh quality, computer operation speed, and solution efficiency take a relatively small amount of computational memory, which can guarantee the grid quality. The mesh of the symmetrical body of the bearing is treated as follows: We determine the grid by using the sweep method, the number of units of thrust bearing diameter is set to 260, and the number of cells is 80 in the film thickness direction, 32 units are taken in symmetrical boundaries. The type of

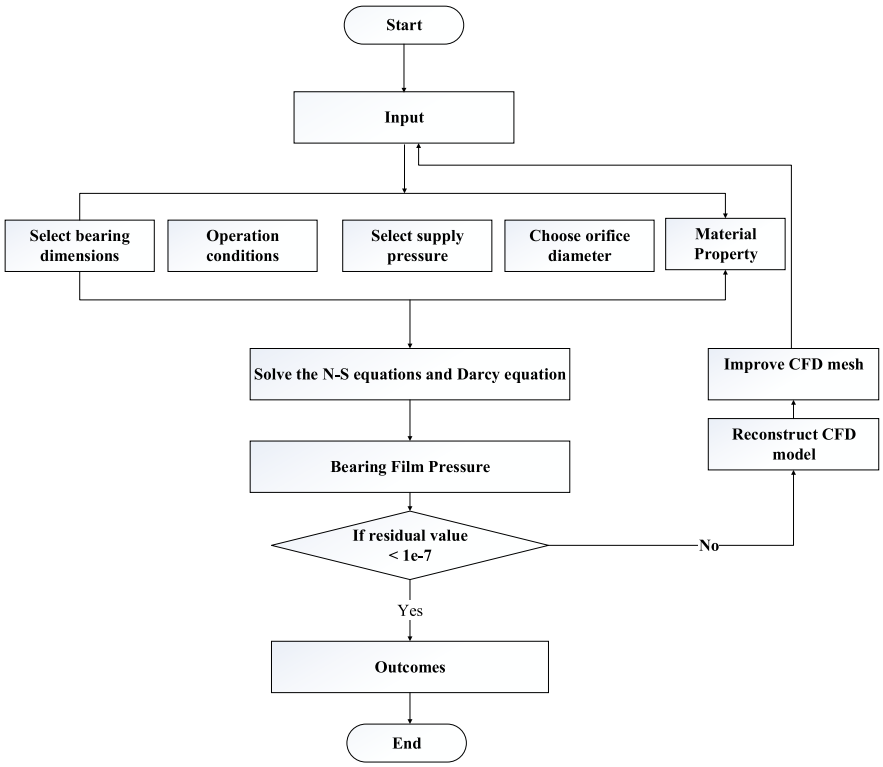

FIGURE 2. The flow chart determining the load capacity and stiffness.

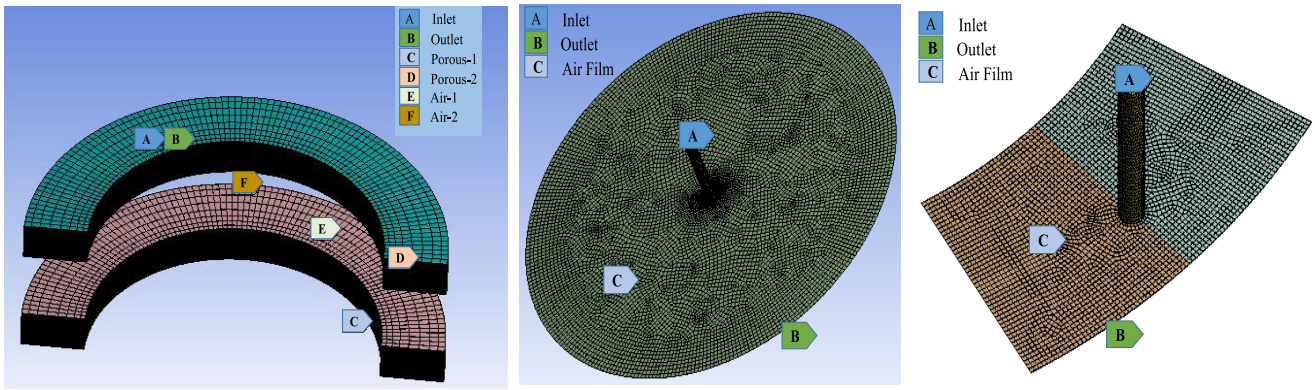

(a) porous (b) orifice (c) multiple orifice

FIGURE 3. Mesh model of aerostatic thrust bearing.

element is used hexahedral mesh, and mesh size is set by default. We have presented the nodes and elements in Table 3. The effect of grid numbers on simulation results is shown in Table 3 under the conditions of pressure supply is $0.4MPa$, the porous thickness is 8mm, and the number of nodes and elements are 520020 and 494160, respectively. The lengths in X, Y, and Z direction are $8.e-002m$,$4.e-002$m,and $6.0045e-003$m, respectively. The volume is $7.6964e-006m$. The numerical convergence parameters in the fluid domain and the different number of iterations are set to get the simulation results, and the results are not affected by using different iterations. We have fixed the same number of iteration to save time. For the convergence criteria, we have set $1e-6$ in residuals of continuity, x, y, and z velocity. Finally, the actual result is obtained into the results module for post-processing. The model is selected as periodic axisymmetric for the orifice restrictors, as depicted in Fig 3, and for the calculations, the slice of the geometric structure is essential. For the computation of the different types of restrictors, the conditions used, as stated in Table 2.

IV. EXPERIMENTAL SETUP

A. TEST OF PERMEABILITY OF POROUS MATERIAL

The permeability co-efficients are majorly effecting on the CFD results and performance of porous bearings. The permeability co-efficient gives consideration throttle performance

TABLE 2. Computational conditions and input parameters of CFD for different restrictors.

Computational conditions and design variable	Value
Viscosity Flow	Laminar
Inertia co-efficient	2.58e+5 1/m
Fluid	Ideal gas
Temperature	293 K
Method of solution	Simple C
Solution standardization	Standard initialization
Atmospheric pressure	101.325 k Pa
Supply pressure	0.4 MPa/ 0.5 MPa/ 0.6 MPa
Specific heat	1.00643 kJ/(kg.K)
Outlet pressure	0 MPa
Inside diameter	56000 μm
Outside diameter	80000 μm
Rows of orifices	1
Location of orifice row	68000 μm
Number of orifices	12
Diameter of orifice	0.05-0.15mm
Co-efficient of viscous resistance	1.27e+14 m-2
Dynamic Viscosity	$1.789e^{-5}$skg/(m-s)
Porosity	0.18
Bearing thickness H	6mm/8mm/10mm
Thickness of gas film	20 μm

TABLE 3. Grid division information of aerostatic thrust bearing.

Object Name	Geometry
State	Fully Defined
Bounding box	
Length X	$8.e-002m$
Length Y	$4.e-002m$
Length Z	$6.0045e-003m$
Properties	
Volume	$7.6964e-006m$
Scale Factor Value	1.
Statistics	
Bodies	2
Active Bodies	2
Nodes	520020
Elements	494160
Mesh Metric	None

Table

of the restrictor, which changes from 10^{-6}m^2 to 10^{-15}m^2. In Fig 4. the porous material is utilized by test equipment to acquire the permeability co-efficient with a diameter of 80mm and thickness of 8mm, porous graphite material is the measured specimen. The test platform comprises on precision pressure regulating valve, gas tank, flowmeter, fixture,

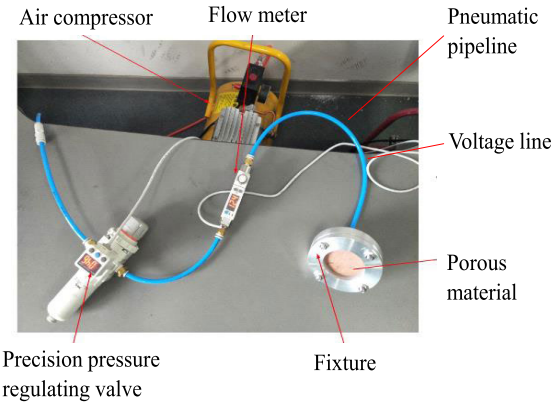

FIGURE 4. Experimental setups for the permeability of porous material.

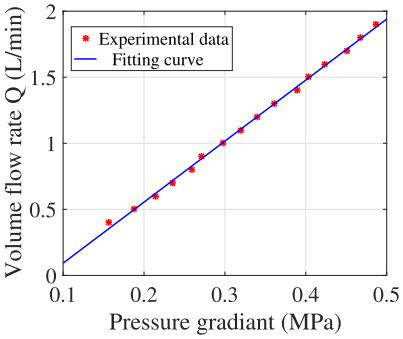

FIGURE 5. The relation of pressure and rate of flow of porous material.

porous material, voltage line, pneumatic pipeline, and dried, pressurizes air supply system, etc.

The air compressor supplies clean gas; the gas storage tank has the purpose of holding stable pressure of the gas, the flow meter is used for calculating volume flow of gas through the porous material. The precision regulating valve has the function of accurately adjusting and reading the pressure. The fixture is used for sealing and supporting the porous material to be tested. The diameter of the inlet area of the fixture is 40mm. The porous material is sealed with epoxy resin to prevent leakage of gas, and then it can be put into water for sealing test.

The gas flow and its flow-rate are measured by the flowmeter. The pressure sensor is used for measuring pressure. The pressure change and flow-rate give the internal flow of the material, as shown in Fig 5.

In Fig 5 relation between change in pressure and rate of flow is linear and fulfills the condition of Darcy-Forchheimer law. The gas flows through porous material governed by the law of Darcy-Forchheimer, given below.

$$\Psi = \frac{Q\eta H}{\Delta pa} \tag{13}$$

where a is the surface area along the direction of gas flow, η is the kinematic viscosity of the gas, Δ_p is the change in pressure between front and back porous material surface,

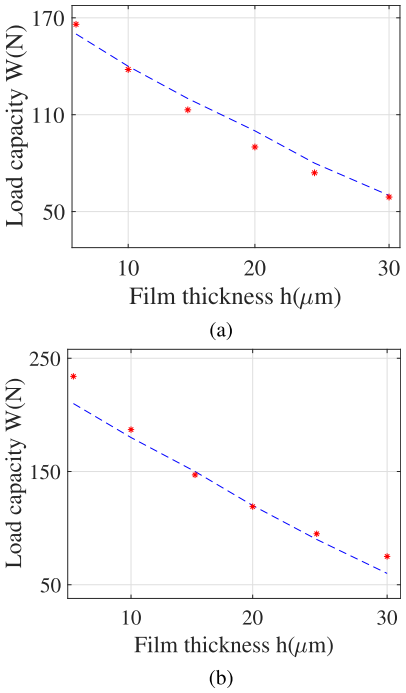

FIGURE 6. Experimental and simulation results of porous aerostatic thrust bearings.

H is the thickness of porous material, and Ψ is the co-efficient of permeability of porous material. Q is volume flow through the porous material.

B. LOAD CAPACITY TESTS OF POROUS THRUST AEROSTATIC BEARINGS

The LCC of porous thrust aerostatic bearings is measured by the experimental setup. For reducing the environmental disruption, the equipment of measurement is put on a platform of vibration isolation. The static performance test platform comprises of load precision pressure regulating valve, porous thrust bearings, fixture, gas tank, flow meter, pneumatic pipeline, etc. The load applied to porous thrust aerostatic bearings is measured by load transducers. The displacement sensors are used to measure a change in the thickness of a film.

V. EXPERIMENTAL VERIFICATIONS WITH NUMERICAL ANALYSIS

A. EXPERIMENTAL VALIDATION

The experimental LCC results of a porous aerostatic bearing are depicted in Fig 6. The experimental results indicate the agreement with simulated results. Therefore, in this paper, we adopt the numerical method for validation purpose.

The 17.11% of LCC of porous aerostatic thrust bearing is the maximum variance between the results of experiments and simulation. The benefit of the porous restrictor is better when the film thickness is below: 5μm. LCC is decreasing with an increase in film thickness, and with the supply of 0.4 MPa pressure. With a 0.5 MPa supply of pressure, the load capacity is more than 0.4MPa

B. NUMERICALLY ANALYSIS

In this study, we choose the viscous laminar, ideal gas model, CFD, and SIMPLEC by using FLUENT software. In Table 2, the boundary conditions and geometrical parameters are given. The LCC of porous aerostatic bearings decreases with the increase of air film thickness, whereas, with increasing thickness of porous, LCC decreases. In contrast, the LCC increases with the rise of supply pressure. The LCC is smaller with a smaller co-efficient of permeability. The LCC gradually decreases when the 15μm is the thickness of a film, while the porous thickness is 6 mm when the thickness of an air film is 5μm, the load is high. For keeping a comparatively high load of bearings under the minimum usage of gas, it requires to reduce a diameter of porous restrictor aerostatic bearing. The load-carrying capacity is delicate to vary in diameter.

As depicted in Fig 8, the aerostatic bearing's stiffness decreases, when the thickness of air film decreases. The porous restrictor thickness can affect the stiffness of aerostatic bearings. The stiffness increases, as the porous restrictor thickness increases. The bearings have different stiffness relative to varying air film thickness. The stiffness is delicate to vary in thickness. The high value of stiffness can be obtained with a large thickness of porous thickness. For determining the porous aerostatic bearing's performance, the material permeability is the key parameter. Generally, it is taken between $10^{-14}m^2$ and $10^{-12}m^2$ [30].

The rate of mass flow increasing with decreasing of porous thickness, as shown in Fig 9. The flow of mass is especially affected by the variation of porous thickness, diameter, and film thickness of porous restrictor, whereas the thickness of the film is more affecting on stiffness. Generally, it is easy to guarantee the accuracy of impact machinery with air film thickness greater than 15μm, but if its restrictor thickness is too low, the restrictor may be damaged. [31]. The boundary conditions for orifice type aerostatic bearings are the same as for porous aerostatic bearings. The static characteristics of orifice type bearings are obtained by using CFD Fluent. In Fig 10, the LCC increases as the thickness of air film decrease, but the bearings have different load-carrying capacity with different diameters of orifice. The LCC increases by increasing the diameter of the orifice; it decreases as the thickness of air film is more than 15μm but increases with increasing air pressure.

With an increase in air film thickness, first, the stiffness increases then decrease, as shown in Fig 11. The different sizes of orifice diameter and the film thickness bring the change in the results of stiffness. The stiffness reduces when the diameter of an orifice is 0.5mm. Moreover, the results also show that the stiffness is high when the thickness of air film is between 5μm and 15μm, and it reduces uniformly after 15μm air film thickness. Furthermore, by taking the less than 100μm diameter of the orifice and less than 10μm thickness of air film is optimal. The reduction in the diameter

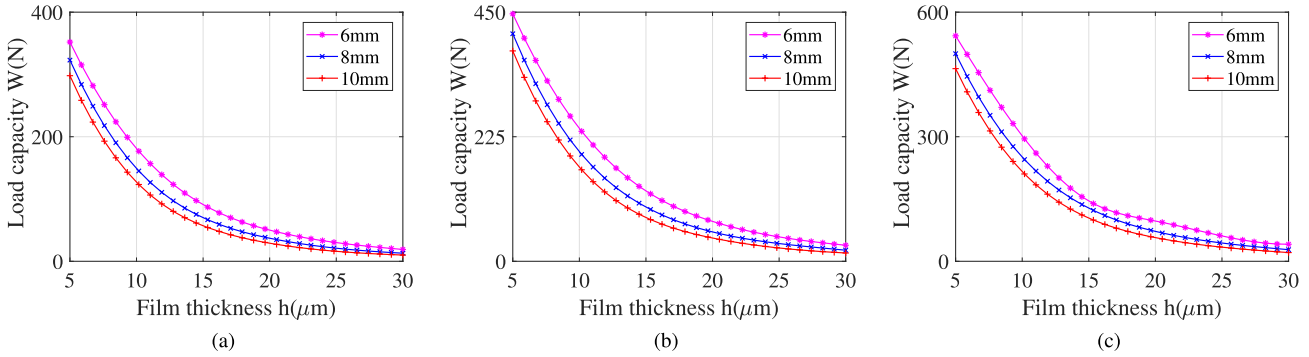

FIGURE 7. Load capacity versus film thickness (h) of porous restrictor of the bearings.

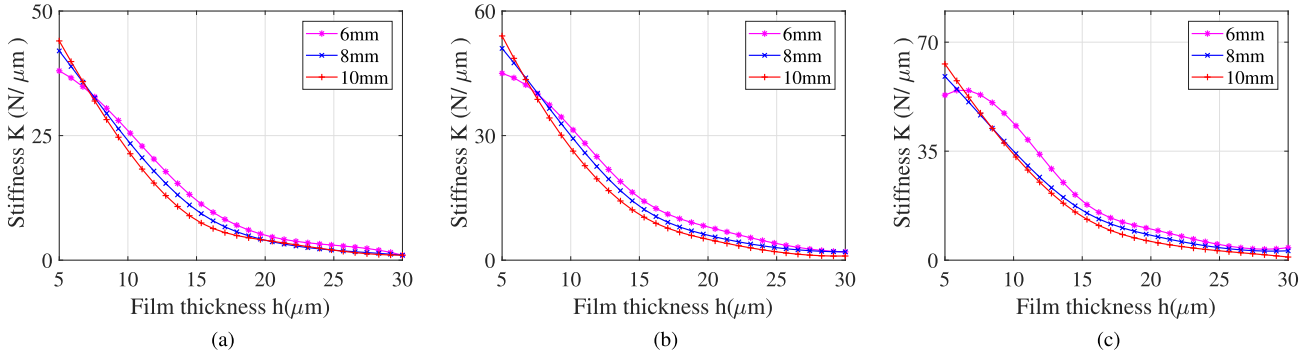

FIGURE 8. Stiffness versus film thickness (h) of porous restrictor of the bearing.

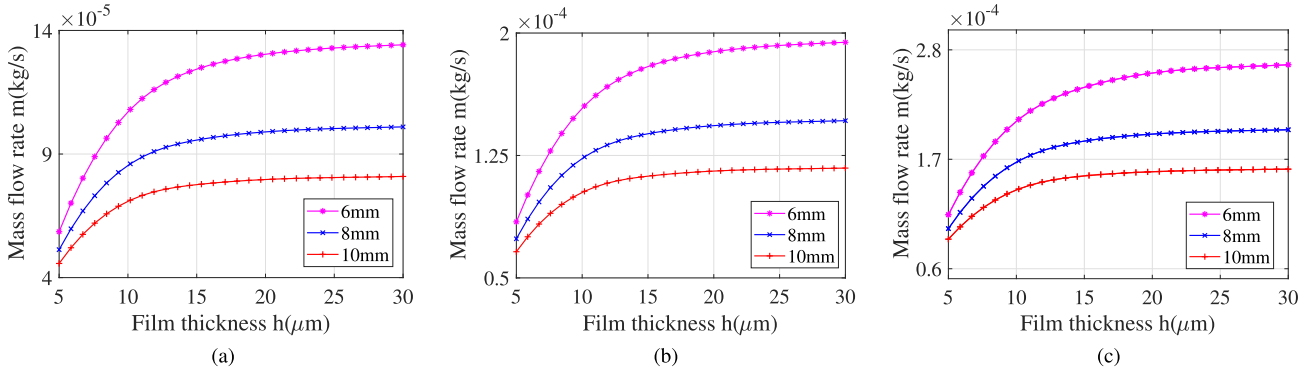

FIGURE 9. Mass flow versus film thickness (h) of porous restrictor of the bearings.

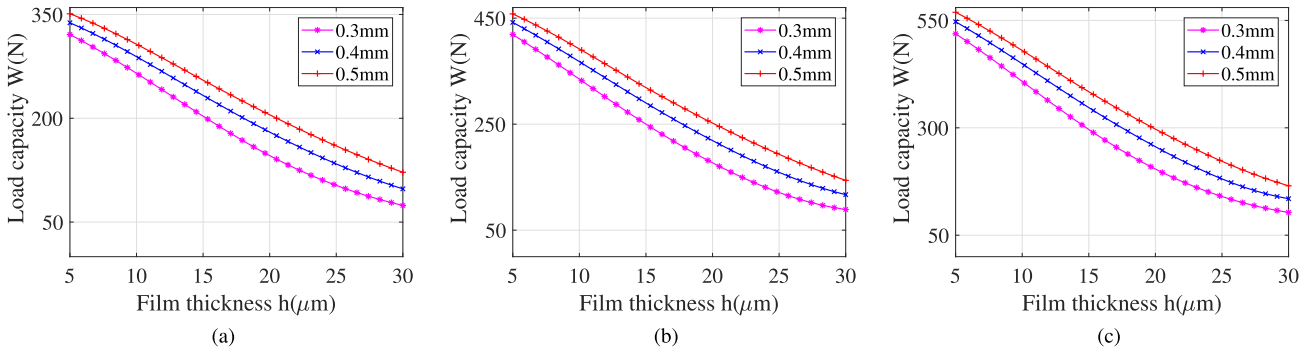

FIGURE 10. Load capacity versus film thickness (h) of orifice restrictor of the bearings.

of orifice and film thickness creates hard processing. In this section, we determine that bearings can take full advantage when working between 10μm and 15μm film thickness. The multiple restrictors are usually designed to upkeep the load of the aerostatic bearing. So, the number of restrictors certainly is the key factor for the bearing objective. In the

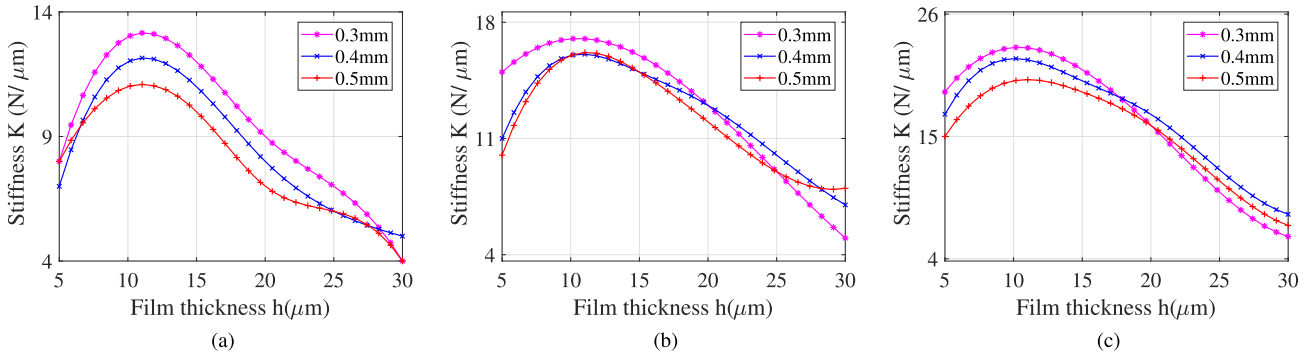

FIGURE 11. Stiffness versus film thickness (h) of orifice restrictor of the bearings.

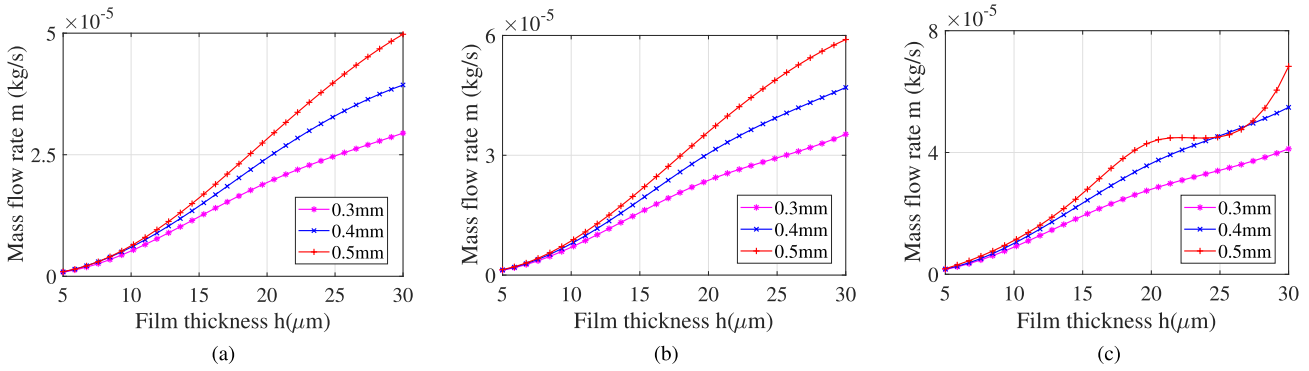

FIGURE 12. Mass flow versus film thickness (h) of orifice restrictor of the bearings.

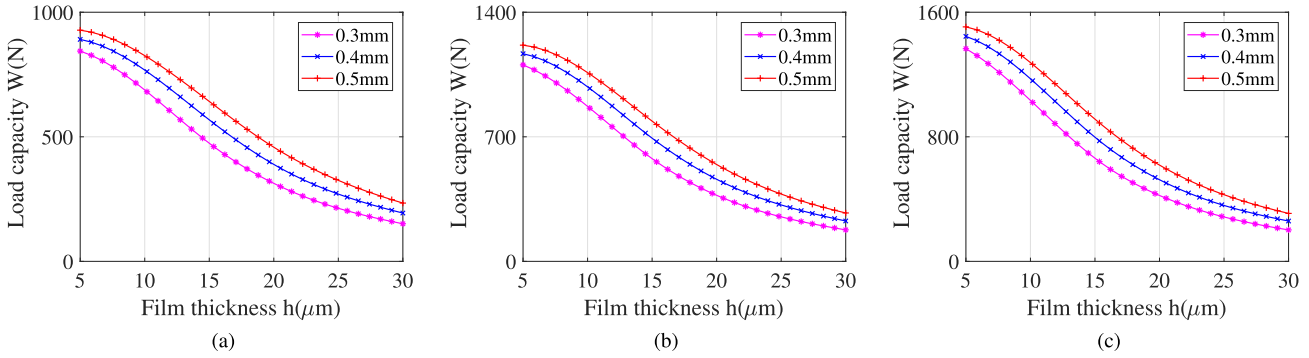

FIGURE 13. Load capacity versus film thickness (h) of multiple orifice restrictor of the bearings.

results, Fig 12 shows that the decrease in air film causes an increase in mass flow. However, an increase in the orifice diameter decreases the mass flow of gas. The 80mm and 56mm are the outside and inside diameters of the aerostatic thrust bearing, respectively. The orifices are placed around a circle of reference diameter of 68mm. We use the similar boundary conditions of multiple orifice restrictors.

The characteristics of aerostatic thrust bearing with multiple orifices as illustrated in Fig 13. However, the LCC of multiple restrictors can increase by increasing the orifice diameter.

It is analysed that the stiffness increases by increasing air film thickness, but it decreases with increasing film thickness (see Fig 14). Whereas the stiffness of aerostatic bearing decreases by increasing the number of orifices, but it rises by reducing the diameter of the orifice. The stiffness of multiple orifices increases by increasing the supply of air pressure, but it is maximum as the air film thickness is between 10μm and 15μm.

The mass flow reaches a high rate due to the maximum pressure supply, but by reducing air film thickness, the consumption of gas is minimum. The increment number of orifices causes the increase of mass flow, as shown in Fig 15. By taking the large orifice diameter, the gas consumption is high, but mass flow decreases as the diameter of orifice decreases.

The comparison of three types of restrictors reveals that the LCC of the porous is 8.8% greater than a single orifice by

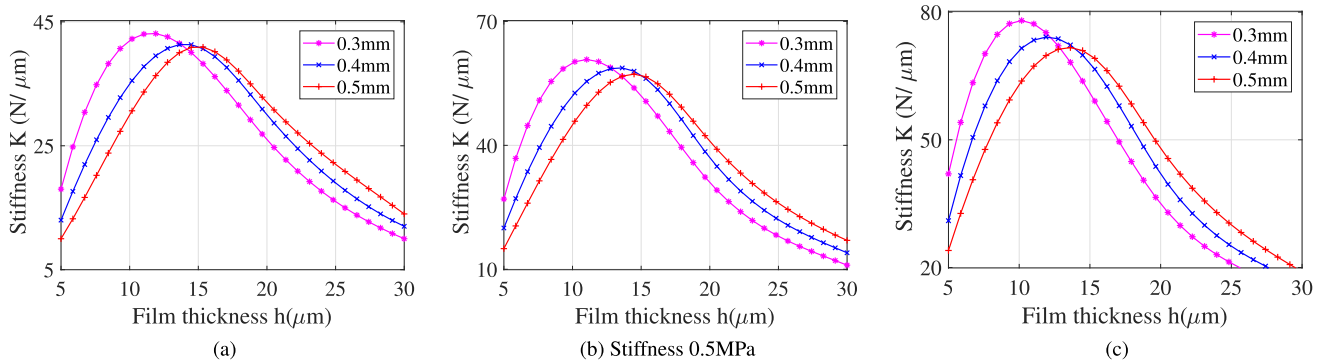

FIGURE 14. Stiffness versus film thickness (h) of multiple orifice restrictor of the bearings.

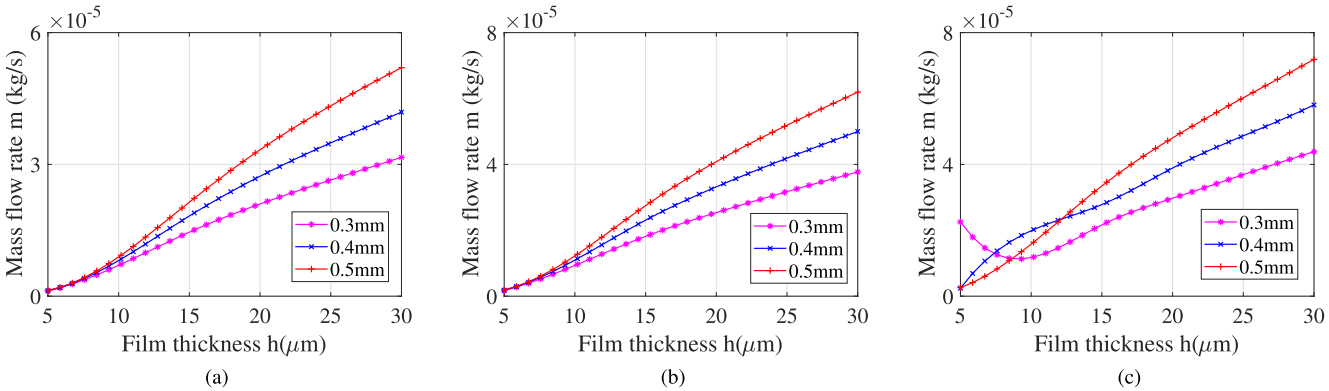

FIGURE 15. Mass flow versus film thickness(h) of multiple orifice restrictor of the bearings.

taking 5μm as the air film thickness. However, the stiffness is similar to the single orifice as the air film thickness is 5μm. The LCC of multiple orifice restrictors is higher than both porous and single orifice restrictor aerostatic bearings. The stiffness is more than the porous bearings by increasing the number of orifices. At the 10μm air film thickness, the stiffnesses are higher than the porous restrictors.

VI. CONCLUSION AND FUTURE WORK

This work investigates the advantages and disadvantages, which are based on the factors optimization of porous and orifice type bearings. Several findings are given as follows:

The stiffness of porous restrictors regularly decreases by reducing the thickness of porous; for single and multiple orifice restrictors, it slowly rises at the highest value of thickness then declines with an increase of thickness of air film. The material and geometrical factors are effecting meaningfully on aerostatic bearing's stiffness.The change in air film thickness influences the stiffness of porous restrictors.

The multiple restrictors have stiffness ominously better than single orifice restrictor. When the thickness of air film is less than 5μm, the porous restrictors have benefits for stiffness. Therefore, the stiffness of porous is better as compared to a single orifice restrictor. When an air film thickness is more than 5μm, the stiffness of multiple restrictors decreases. The LCC of multiple orifice restrictors is larger than porous and single orifice restrictors. The multiple orifice restrictors have more load capacity than porous and single orifice restrictor as the air film thickness is less than 10μm. By increasing pressure of the gas, the stiffness and LCC of porous, single, and multiple orifice restrictors can be better. The material thickness and supply of pressure are affecting LCC, stiffness of porous, single, and multiple orifice restrictors. However, by increasing the diameter of multiple orifice restrictor, the stiffness of aerostatic thrust bearing is improved. This research work is based on the experimental and simulation design of porous aerostatic thrust bearing. Simulation is performed for orifice and multiple orifice aerostatic thrust bearing. In the future, we aim to conduct an experimental study on the orifice and multiple orifice restrictor bearings.

REFERENCES

[1] U. Nishio, K. Somaya, and S. Yoshimoto, "Numerical calculation and experimental verification of static and dynamic characteristics of aerostatic thrust bearings with small feedholes," *Tribol. Int.*, vol. 44, no. 12, pp. 1790–1795, Nov. 2011.

[2] H. Cui, Y. Wang, X. Yue, M. Huang, W. Wang, and Z. Jiang, "Numerical analysis and experimental investigation into the effects of manufacturing errors on the running accuracy of the aerostatic porous spindle," *Tribol. Int.*, vol. 118, pp. 20–36, Feb. 2018.

[3] J. Zhang, D. Zou, N. Ta, and Z. Rao, "Numerical research of pressure depression in aerostatic thrust bearing with inherent orifice," *Tribol. Int.*, vol. 123, pp. 385–396, Jul. 2018.

[4] M. Huang, Q. Xu, M. Li, B. Wang, and J. Wang, "A calculation method on the performance analysis of the thrust aerostatic bearing with vacuum pre-load," *Tribol. Int.*, vol. 110, pp. 125–130, Jun. 2017.
[5] S. Yoshimoto and K. Kohno, "Static and dynamic characteristics of aerostatic circular porous thrust bearings (effect of the shape of the air supply area)," *J. Tribol.*, vol. 123, no. 3, pp. 501–508, Jul. 2001.
[6] Y. Li and H. Ding, "A simplified calculation method on the performance analysis of aerostatic thrust bearing with multiple pocketed orifice-type restrictors," *Tribol. Int.*, vol. 56, pp. 66–71, Dec. 2012.
[7] C. Schenk, S. Buschmann, S. Risse, R. Eberhardt, and A. Tünnermann, "Comparison between flat aerostatic gas-bearing pads with orifice and porous feedings at high-vacuum conditions," *Precis. Eng.*, vol. 32, no. 4, pp. 319–328, 2008.
[8] Y. R. Jeng and S. H. Chang, "Comparison between the effects of single-pad and double-pad aerostatic bearings with pocketed orifices on bearing stiffness," *Tribol. Int.*, vol. 66, pp. 12–18, Oct. 2013.
[9] H. Cui, Y. Wang, X. Yue, M. Huang, and W. Wang, "Effects of manufacturing errors on the static characteristics of aerostatic journal bearings with porous restrictor," *Tribol. Int.*, vol. 115, pp. 246–260, Nov. 2017.
[10] Y. Hechun, L. Huanhuan, Z. Huiying, and M. Wenqi, "Research on the static characteristics of circular thrust porous aerostatic bearings," in *Proc. IEEE Int. Conf. Mechatronics Autom. (ICMA)*, Aug. 2015, pp. 1407–1411.
[11] H. Cui, Y. Wang, H. Yang, L. Zhou, H. Li, W. Wang, and C. Zhao, "Numerical analysis and experimental research on the angular stiffness of aerostatic bearings," *Tribol. Int.*, vol. 120, pp. 166–178, Apr. 2018.
[12] W. Wang, X. Cheng, M. Zhang, W. Gong, and H. Cui, "Effect of the deformation of porous materials on the performance of aerostatic bearings by fluid-solid interaction method," *Tribol. Int.*, vol. 150, Oct. 2020, Art. no. 106391.
[13] M. Miyatake and S. Yoshimoto, "Numerical investigation of static and dynamic characteristics of aerostatic thrust bearings with small feed holes," *Tribol. Int.*, vol. 43, no. 8, pp. 1353–1359, Aug. 2010.
[14] W.-J. Lin, J. P. Khatait, W. Lin, and H. Li, "Modelling of an orifice-type aerostatic thrust bearing," in *Proc. 9th Int. Conf. Control, Autom., Robot. Vis.*, 2006, pp. 1–6.
[15] Y. B. P. Kwan and J. Corbett, "Porous aerostatic bearings—An updated review," *Wear*, vol. 222, no. 2, pp. 69–73, Nov. 1998.
[16] M. Fourka and M. Bonis, "Comparison between externally pressurized gas thrust bearings with different orifice and porous feeding systems," *Wear*, vol. 210, nos. 1–2, pp. 311–317, Sep. 1997.
[17] T. S. Luong, W. Potze, J. B. Post, R. A. J. van Ostayen, and A. van Beek, "Numerical and experimental analysis of aerostatic thrust bearings with porous restrictors," *Tribol. Int.*, vol. 37, no. 10, pp. 825–832, Oct. 2004.
[18] Y. Tian, "Static study of the porous bearings by the simplified finite element analysis," *Wear*, vol. 218, no. 2, pp. 203–209, Jul. 1998.
[19] A. Charki, K. Diop, S. Champmartin, and A. Ambari, "Numerical simulation and experimental study of thrust air bearings with multiple orifices," *Int. J. Mech. Sci.*, vol. 72, pp. 28–38, Jul. 2013.
[20] A. Hakeem, M. Nayak, and O. Makinde, "Effect of exponentially variable viscosity and permeability on blasius flow of carreau nano fluid over an electromagnetic plate through a porous medium," *J. Appl. Comput. Mech.*, vol. 5, no. 2, pp. 390–401, 2019.
[21] M. K. Moayyedi, "Extension ability of reduced order model of unsteady incompressible flows using a combination of pod and Fourier modes," *J. Appl. Comput. Mech.*, vol. 5, no. 1, pp. 1–12, 2019.
[22] M. Delkhosh, K. Parand, and D. D. Ganji, "An efficient numerical method to solve the boundary layer flow of an eyring-powell non-newtonian fluid," *J. Appl. Comput. Mech.*, vol. 5, no. 2, pp. 454–467, 2019.
[23] B. Fallah, S. Dinarvand, M. Eftekhari Yazdi, M. N. Rostami, and I. Pop, "MHD flow and heat transfer of SiC-TiO_2/DO hybrid nanofluid due to a permeable spinning disk by a novel algorithm," *J. Appl. Comput. Mech.*, vol. 5, no. 5, pp. 976–988, 2019.
[24] M. Shamshuddin, T. Thirupathi, and P. Satya Narayana, "Micropolar fluid flow induced due to a stretching sheet with heat source/sink and surface heat flux boundary condition effects," *J. Appl. Comput. Mech.*, vol. 5, no. 5, pp. 816–826, 2019.
[25] H.-L. Cui, Y. Wang, B.-R. Wang, H. Yang, and H. Xia, "Numerical simulation and experimental verification of the stiffness and stability of thrust pad aerostatic bearings," *Chin. J. Mech. Eng.*, vol. 31, no. 1, pp. 1–12, Dec. 2018.
[26] J. W. Powell, *Design of Aerostatic Bearings*. London, U.K.: The Machinery Publishing Co.Ltd., 1970.
[27] L. Song, K. Cheng, H. Ding, and S. Chen, "Analysis on discharge coefficients in FEM modeling of hybrid air journal bearings and experimental validation," *Tribol. Int.*, vol. 119, pp. 549–558, Mar. 2018.
[28] J. Huang, J. Zhang, W. Shi, and Y. Wang, "3D FEM analyses on flow field characteristics of the valveless piezoelectric pump," *Chin. J. Mech. Eng.*, vol. 29, no. 4, pp. 825–831, Jul. 2016.
[29] X.-D. Chen and X.-M. He, "The effect of the recess shape on performance analysis of the gas-lubricated bearing in optical lithography," *Tribol. Int.*, vol. 39, no. 11, pp. 1336–1341, 2006.
[30] L. Zesheng, D. Jinming, and S. Yazhou, "Analysis on aerostatic porous spherical bearings static performance," *Chin. J. Mech. Eng.*, vol. 40, pp. 115–119, 2004.
[31] X. F. Zhang and B. Lin, "Theoretical research on deformation of porous material in air bearing," *Appl. Mech. Mater.*, vols. 215–216, pp. 779–784, Nov. 2012.

MUHAMMAD PUNHAL SAHTO was born in Pakistan, in January 1983. He received the B.E. degree from the Department of Mechanical Engineering, Quaid-E-Awam University of Engineering, Science and Technology, Nawab Shah, Pakistan, and the master's degree in mechanical engineering from UET Lahore, Pakistan. He is currently pursuing the Ph.D. degree with the School of Mechanical and Electrical Engineering, University of Electronic Science and Technology of China (UESTC).

He is also as an Assistant Professor with the Department of Mechanical Engineering, The University of Lahore, Pakistan. His research interests include fluid mechanics, mechanical design engineering, and mechanical systems.

WEI WANG is currently a Professor with the School of Mechanical and Electrical Engineering, University of Electronic Science and Technology of China (UESTC). His research interests include digital design, simulation, and manufacturing, detection, control, and automation of manufacturing equipment.

MUHAMMAD IMRAN is currently working as a Lecturer with Aston University, U.K. He is also an Established Researcher in the area of thermal energy systems. His research interests include developing innovative thermal energy systems and improving the energy performance of existing energy systems.

LINSHAN HE received the M.S. degree in mechanical engineering from the University of Electronic Science and Technology of China (UESTC).

His research interests include air static pressure bearings and fluid simulation.

HAI LI received the M.S. degree in mechanical engineering from the University of Electronic Science and Technology of China (UESTC), China, where he is currently pursuing the Ph.D. degree with the School of Mechanical and Electrical Engineering. His research interests include machine learning, data mining, machinery working condition monitoring, and production scheduling.

GONG WEIWEI received the bachelor's degree in mechanical engineering from the University of Electronic Science and Technology of China (UESTC), where he is currently pursuing the master's degree.

His research interests include computational fluid dynamics, aerostatic bearing, and lapping machine.